EXTENDING THE GRS DRY STROAGE SIMULATION CHAIN TO ANALYSE BWR STORAGE CASK INVENTORY

Daniel Nahm
Gesellschaft für Anlagen- und Reaktorsicherheit (GRS) gGmbH
Boltzmannstr. 14, 85748 Garching
Daniel.nahm@grs.de

Felix Boldt, Volker Hannstein and Robert Kilger
Gesellschaft für Anlagen- und Reaktorsicherheit (GRS) gGmbH
Boltzmannstr. 14, 85748 Garching

ABSTRACT

Predictions of safety-relevant parameters for spent nuclear fuel (SNF) during storage require detailed knowledge about the thermo-mechanical behaviour of the fuel rods. Detailed assessments need to consider the entire life cycle of the fuel rod, ranging from fabrication, in-reactor irradiation, over wet storage and finally to dry storage. Here we present the temperature field simulation for a generic boiling water reactor (BWR) storage and transportation cask over a period of 100 years using COBRA-SFS. Applying these results as boundary condition, the fuel rod performance code TESPA-ROD was applied to predict the thermo-mechanical behaviour of the fuel rod experiencing the highest thermal load.

INTRODUCTION

Fuel rods face considerable changes in the environmental conditions during their life cycle, including reactor operation and storage. Examples are varying pressure gradients, alternating heat loads and ongoing decay processes in the spent nuclear fuel (SNF). For the simulation of important parameters for the safety assessment of SNF storage, GRS uses a simulation chain of COBRA-SFS and TESPA-ROD [1]. The COBRA-SFS code, as a validated simulation tool, is used to perform the calculation of the thermo-hydraulic boundary conditions [2]. It is coupled to the GRS in-house fuel rod code TESPA-ROD which uses these conditions for the simulation of cask-based dry storage and allows predicting thermo-mechanical parameters of single fuel rods [3]. Currently, this calculation chain includes two generic pressurized water reactor (PWR) cask models similar to a CASTOR V/19 and a TN-32B, which enables general predictions for the behaviour of PWR fuel rods during extended storage.

However, with respect to heavy metal mass, about one third of the German light water reactor (LWR) inventory are boiling water reactor (BWR) fuel assemblies (FAs). Therefore, this assembly type is also of interest for safety assessment, especially in the context of the upcoming extension of dry storage time in Germany. Since BWR FAs in Germany are usually stored in the CASTOR® V/52 cask, we developed a generic COBRA-SFS model similar to this cask type. Using this model, the temperature field for loading scenarios with varying thermal heat load was predicted and critical parameters for the safety assessment of SNF storage, such as the hoop stress and the creep strain in the fuel rod cladding, were calculated.

Calculation model

The generic cask model of the CASTOR® V/52 was developed within the thermo-hydraulic code COBRA-SFS cycle 4a and includes a detailed structure of the cask as well as an explicit model of the FAs. Heat exchange via thermal conduction throughout the solid cask structure as well as all helium-filled void channels and thermal radiation through open spaces and gaps are permitted. Furthermore, the heat transfer via natural helium convection, within helium channels and the FAs, is taken into account. Figure 1 a) shows a one-fourth cross-section of the symmetric cask model. Note that the structures in this figure are not to scale, but have been enlarged for the purpose of illustration. For this

model, the internal basket structure, the aluminium support rails, helium channels, and FA channels were subdivided into more than 1000 nodes. In axial direction, the cask consists of 36 zones. The outer basket rails are considered as structures of aluminium alloy, whereas the basket is composed out of either stainless steel or a composite with a stainless-steel mantle and an inner liner of aluminium alloy.

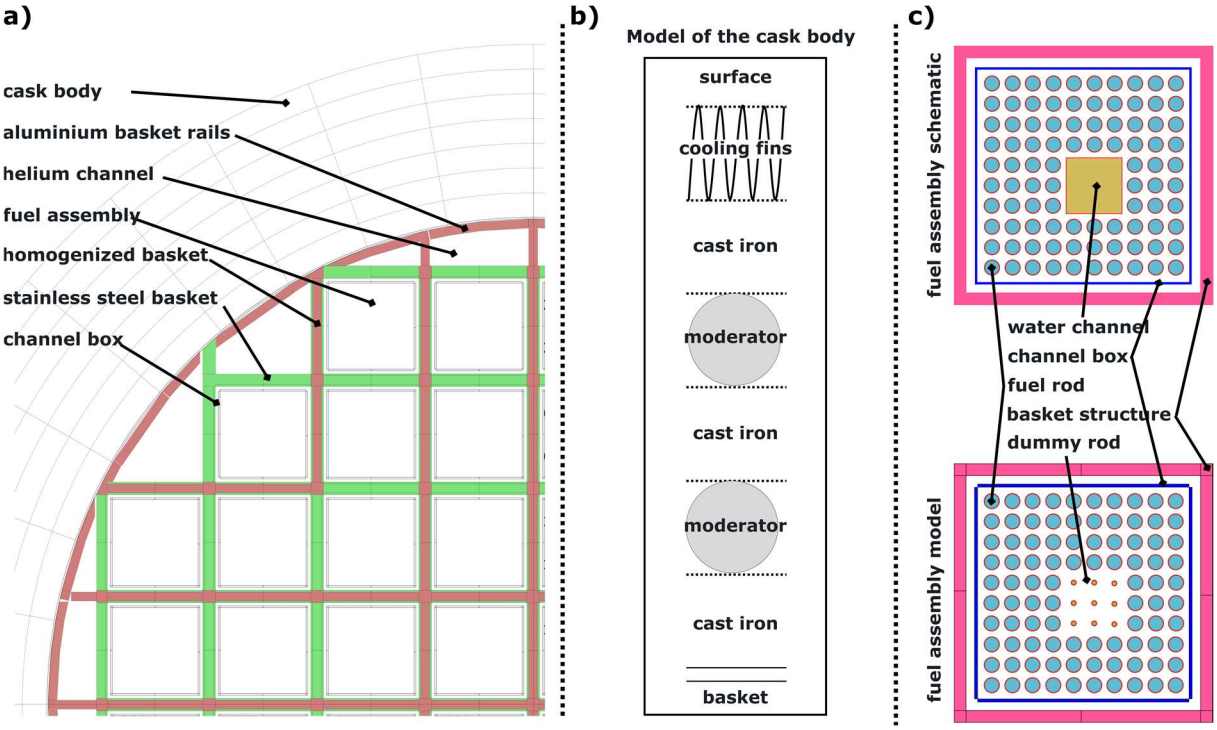

Figure 1: a) One-fourth section of the symmetric CASTOR® V/52 model. b) Detailed description of the mantle structure. c) Schematic illustration of a 10x10 BWR FA (top). Illustration of the implementation of the FA in the COBRA-SFS model (bottom).

For simplicity reasons, these steel aluminium composite structures are modelled as one homogenised material. In the model, the cask body consists of an of heterogenous material structure of cast iron and polyethylene (moderator rods) and was divided into eight radial zones (Figure 1 b)). The sections which contain moderator rods are modelled as a homogenised mixture of both materials. Furthermore, the cask model comprises an upper and lower plenum model which enables a more realistic gas communication throughout the cask cavity. COBRA-SFS allows for the explicit modelling of the FAs in the cask with no need for homogenisation of the rod bearing zone. We considered the cask to be loaded with 10x10 BWR FAs which are shown in figure 1 c) (top part). Each FA consists of the fuel rod bundle with 91 rods, which is surrounded by a channel box, and a water channel in the middle of the grid. BWR FAs often contain partial-length rods, which are not considered in this model. Because of the large water channels displacing several rods in the grid, the implementation of BWR FAs in COBRA-SFS still requires some adaptation. Hence, these channels were approximated with a set of nine small dummy rods (roughly 1/6 of the fuel rod diameter) with zero decay power (Figure 1 c)), bottom part). This, on the one hand, allows straight forward implementation into COBRA-SFS but on the other hand (partially) considers the increased space for helium convection through the water channel. The fuel rod grid is surrounded by eight nodes, which represent the channel box.

Results

Simulation of the temperature during prolonged storage

Typical generic burn-up profiles for 10x10 BWR UO_2 FAs with a burn-up of 55 GWd/tHM and 65 GWd/tHM (Figure 2 a)) as well as generic power histories were used for the calculation of the decay heat with the GRS in-house nuclide inventory and source term calculation code MOTIVE [4].

The resulting decay heat profiles for the FAs as well as the evolution of the assembly average decay heat over a period of 100 years are shown in figure 2 a) and b). These calculations gave assembly averaged decay heat values of 479 W for a burn-up of 55 GWd/tHM and 598 W for a burn-up of 65 GWd/tHM after a decay time of five years. Based on this calculation, three different scenarios were considered (Figure 2 c)). Scenario 1 represents a best estimate homogenous loading of 52 FAs with a burn-up of 55 GWd/tHM and a decay heat as calculated by MOTIVE (total loading 24.9 kW). The scenario 2 assumes the same symmetry, but the assembly averaged decay heat was scaled linearly to match a total cask loading of 40 kW. This matches the total decay heat design limit of a CASTOR® V/52 and represents a conservative scenario [5]. Scenario 3 is a best estimate heterogeneous loading of FAs with a burn-up of 55 and 65 GWd/tHM (total loading 26.8 kW) to evaluate the effect of high burn-up fuel on the temperature field in the cask.

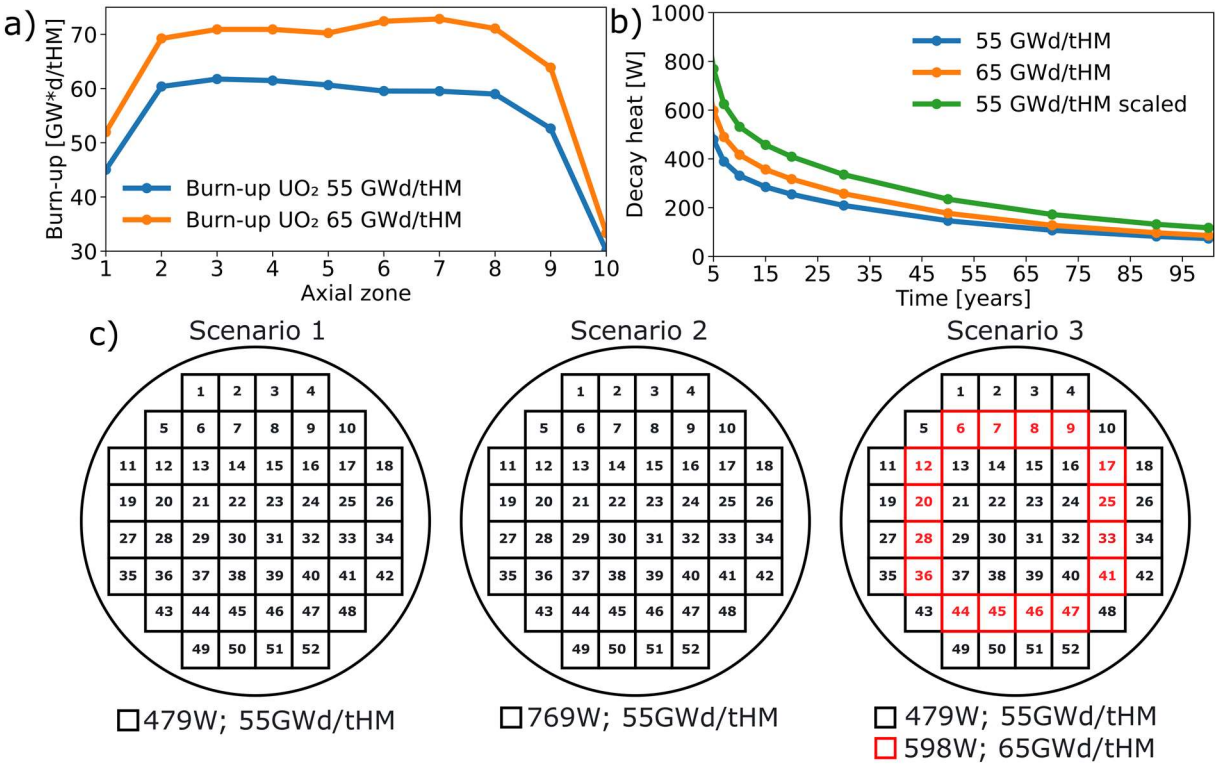

Figure 2: a) Burn-up profiles and b) evolution of the assembly averaged decay heat over 100 years of two generic BWR 10x10 FAs with an average burn-up of 55 GWd/tHM and 65 GWd/tHM. c) Schematic illustration of three generic loading scenarios of a CASTOR® V/52 cask.

Using CORBA-SFS, the temperature field evolution in the generic BWR cask model over a period of 100 years was calculated for the three scenarios. The evolution of the peak cladding temperature (PCT) is displayed in figure 3 a), which reveals temperatures much lower than the German technical PCT limit of 370 °C for all scenarios [6]. The best estimate scenario 1 results, with a PCT of 180 °C after five years of storage, in the lowest temperature. Here, the rods with the highest temperatures are located in the central FAs 22, 23, 30 and 31. In comparison, scenario 3, which includes the FAs with a burn-up of 65 GWd/tHM, results in a higher PCT of 195 °C in the central FAs. In addition, the heterogeneous loading with high burn-up FAs also result in a less steep temperature field over the cask cross-section. For example, the off-centre FA 7 in scenario 1 has a peak temperature of 176 °C whereas FA 7 in scenario 3 shows a temperature of 191 °C. Note, that the temperatures of FA 22 and FA 7 in scenarios 1 and 3 are almost identical over the simulation time period (Figure 3 a)). Scenario 2 results, with a PCT of 272 °C in the innermost FAs, in the highest temperatures of all three cask loadings. The axial temperature profiles for the scenarios 1 to 3 are shown in figure 3 b). The temperature maximum is located slightly above the cask centre, and the lowest temperature can be found at the FA bottom end piece.

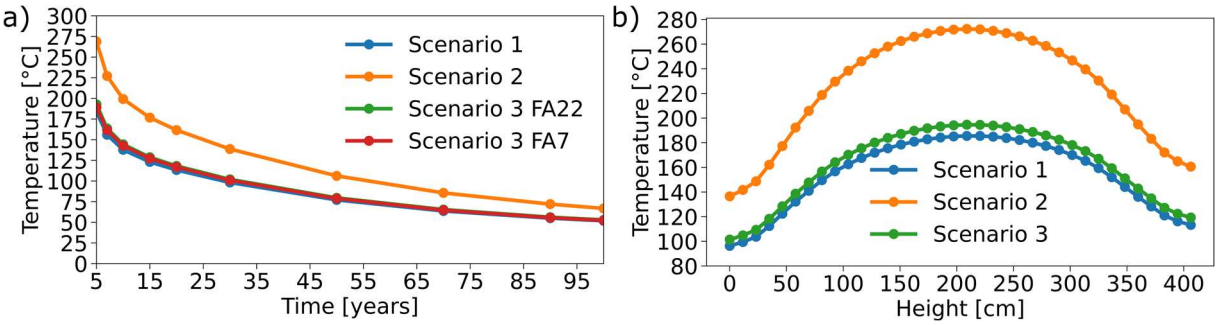

Figure 3: a) Evolution of the peak cladding temperature over 100 years for the scenarios 1 to 3. b) Axial temperature profile of the hottest rod in the cask with a decay time of five years.

A three-dimensional visualisation of the temperature field of the full cask of scenario 2 at a decay time of five years is shown in figure 4. The horizontal cross section through the hottest axial position reveals a temperature gradient from the outermost FA to the innermost FA from 200 °C to 270 °C. Noteworthy is also the effect of the water channels inside the FAs, which allow for heat transport from hot zones to cold zones at the cask top. Since the thin dummy rods in the channel generate no decay heat, the channels are spots of lower temperature located in the hot axial zones and towards the bottom of the cask (Figure 4, vertical slice right side). Yet at higher axial positions the water channels appear as hot spots in their respective FA (Figure 4, vertical slice left side). This can be explained by increased convection enabled by the reduced hydraulic resistance in the water channels, which allows for additional heat transfer from the hotter axial levels to cooler parts near the cask's upper plenum. The COBRA-SFS results support this assumption since the helium velocity in the water channel of one of the hottest FAs (FA 22) is with 1.12 m/s almost two orders of magnitude higher compared to the velocity in space between adjacent fuel rods (0.02 m/s). For scenario 1 the surface of the cask shows the highest temperature of 65 °C at a height of 2 m and the lowest temperature of 53 °C at the cask's top. These temperatures increase for the scenario 2 where the lowest cask surface temperature is 68 °C, and the highest is 85 °C.

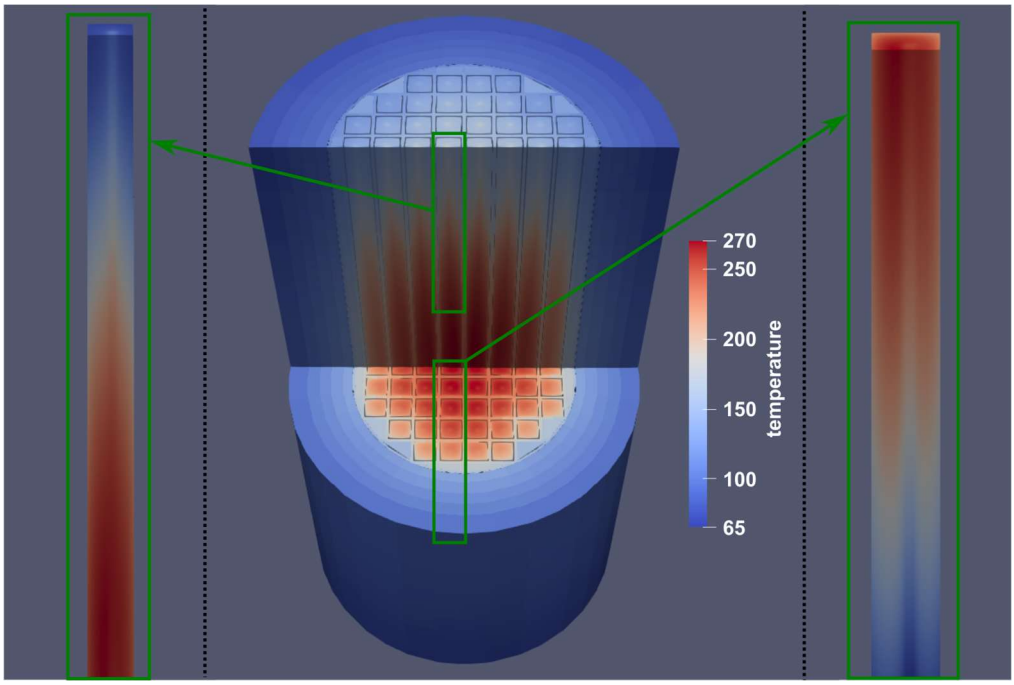

Figure 4: Three-Dimensional visualisation of the temperature field of the cask model in scenario 2 with a decay time of five years. The images on the left and right show a vertical slice through FA 22 at the positions highlighted with the green rectangle.

Prediction of the fuel rod behaviour

The cladding temperature is one of the most influential parameters for predicting safety-relevant parameters for the fuel rod behaviour during dry storage. COBRA-SFS predicted the highest temperatures for scenario 2 and therefore the TESPA-ROD simulation was only performed for the hottest rod in this scenario. Regarding temperature, this scenario bounds the other two scenarios as it is the most demanding environment. The Zircaloy-2 cladding was estimated with an outer diameter of 10,05 mm and a cladding thickness by 0.605 mm as fabricated. The considered storage setting includes the reactor shutdown, five years of forced wet cooling at 45 °C and the following 100 years of dry storage.

TESPA-ROD predicts a re-opening of the before closed fuel cladding gap up to a width of 14 µm at the beginning of the force cooling phase (Figure 5 a)). However, re-opening to such an extent is expected to be unlikely due to a strong bonding of fuel and cladding developed at higher burn-up [7]. Up to now, such interactions are not implemented in TESPA-ROD. With the beginning of dry storage and the accompanied increase of temperature, the gap width is reduced to 12 µm. This reduction is solely due to the higher thermal expansion coefficient of the fuel compared to the cladding. With decreasing temperature, the gap gradually increases over the simulation period of 100 years.

The hoop stress in the cladding is a critical factor for the safety assessment during dry storage. In this generic storage setting, TESPA-ROD simulates a maximum value of 17 MPa (Figure 5 b)). This value is far below the acceptance criterion of 120 MPa, where systematic cladding failure might occur [6]. Also, since there is no gap closure predicted, the hoop stress is only affected by the inner gas pressure, which peaks at 23 bar at the beginning of dry storage. From this point, the pressure gradually decreases due to the cool-down of the storage cask. Yet, after around 40 years, the inner pressure starts to increase again (Figure 5 b)). This is caused by the release of alpha-decay generated helium from the pellet. While TESPA-ROD predicts a constant release rate of helium during the full period of dry storage, in the first years, this effect does not overcome the overall pressure decrease due to the decreasing cask temperature. Both the pressure and the hoop stress are lower than what was found for PWR FAs in a similar scenario [1]. For a fuel rod, the inner pressure is generally governed by the manufacturing pressure, the fission gas release during operation, the helium release due to alpha decay during long term storage as well as the cladding temperature [7]. Considering a similar power history and burn-up, the fission gas release and helium release of BWR and PWR assemblies are expected to be comparable, while the filling pressure from manufacturing is considerably higher for PWR fuel rods [8].

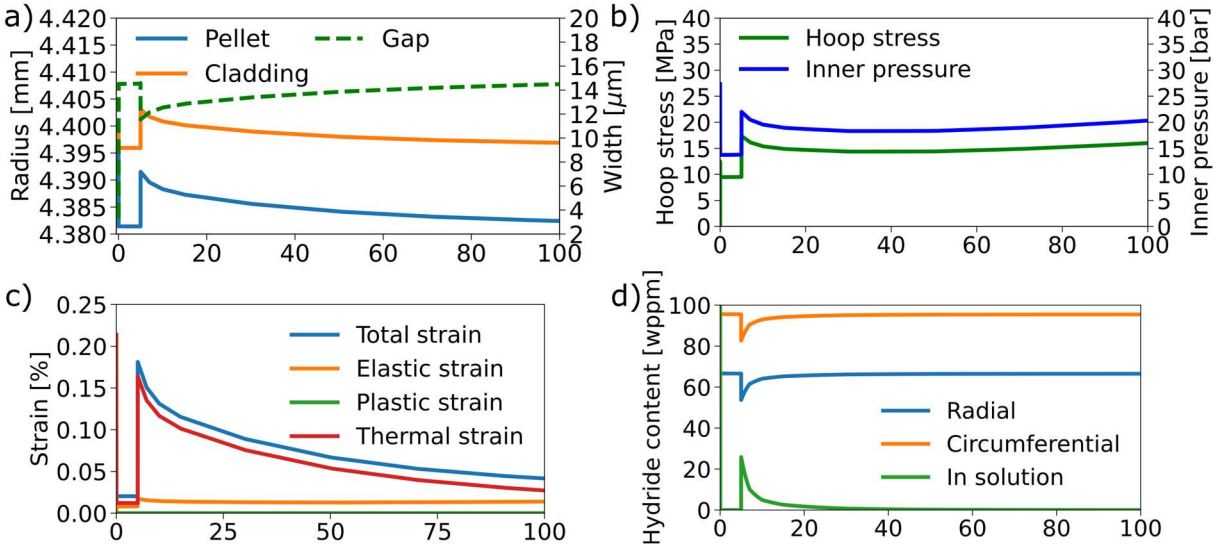

Figure 5: a) Geometric changes, b) pressure and cladding hoop stress, c) cladding strain and d) hydride orientation during the transient.

The total cladding strain is another important criterion for a safety assessment of the fuel rod during dry storage. Generally, to prevent a systematic cladding failure, it is agreed to limit cladding strain to 1 % of its original dimension [6]. Similar to the hoop stress and the inner pressure, the total strain reaches a peak value of 0.18 % with the beginning of dry storage (Figure 5 c)). Note that the strain is mostly caused

by thermal expansion of the cladding, and therefore decreases continuously with progressing storage time. Only a very minor fraction is elastic strain, and no irreversible plastic strain can be observed. Since cladding deformation is most pronounced at high temperature and high inner pressure, these strain values can be attributed to the low inner pressure and the average PCT predicted for this scenario. Another relevant parameter is the hydride orientation in the cladding. In this context, a radial orientation of hydrides may lead to significant weakening of the cladding [9]. When the temperature in the cladding falls below the hydride precipitation temperature, TESPA-ROD calculates the fraction of radial hydrides based on the hoop stress and the temperature gradient over the cladding [10]. At the beginning of the simulation, with reactor shutdown, roughly one third of the hydrides are precipitated in radial orientation (Figure 5 d)). Due to the forced constant low temperature, no changes are observed during wet storage. With the beginning of dry storage, around 30 wppm of hydrides are dissolved in the cladding due to the increase in temperature. This fraction then gradually precipitates during the first 15 years of dry storage. Since neither the temperature gradient nor the hoop stress is high enough, the hydrides are precipitated in no preferred direction, which is assumed to be a 50:50 ratio in the underlying model.

CONCLUSION

The development of a generic BWR cask model extends the GRS calculation chain for the analysis of SNF behaviour during storage. The new model allows for the detailed simulation of the temperature field for different BWR loading scenarios. In all scenarios investigated here, the PCT remained at moderate levels, and the highest temperature of 272 °C was reached for a conservative homogenous cask loading at the design limit of a CASTOR® V/52. Using the temperature field as boundary condition, parameters relevant for the evaluation of the cladding behaviour during storage were calculated. Considering the capabilities of TESPA-ROD for the simulation of dry storage scenarios, the results presented here predict a less demanding environment for the storage of BWR SNF as compared to PWR SNF [1]. This was attributed to the lower rod inner pressure as well as the lower PCT found for the BWR scenarios. However, due to the lack of detailed information on structure and material of a BWR storage cask, the PCT presented here are subject to an unknown degree of uncertainty. The extent of the temperature uncertainty and the sensitivity of this BWR cask model on the input parameters is currently under investigation. Furthermore, there are several phenomena with a potential impact on the integrity of a fuel rod during storage, some of which are still not fully understood today. Examples are fuel swelling during dry storage [11], the reorientation process of hydrides [9] or delayed hydride cracking [12]. These processes might reduce the damage threshold of the cladding significantly, hence further investigations are required to accurately implement these phenomena in fuel rod performance codes for a more accurate long-term prediction.

REFERENCES

[1] F. Boldt, M. Péridis, M. Stuke, *Kerntechnik* **2020**, *85*, 426.
[2] T. E. Michener, D. R. Rector, J. M. Cuta, H. E. Atkins, JR., PNNL-24841, PNNL, **2017**.
[3] GRS, “Fuel Rod Code TESPA-ROD Description”, accessed Apr. 04, **2022**, https://www.grs.de/en/research-and-assessment/reactor-safety/tespa-rod-temperature-strain-and-pressure-analysis-fuel-rod.
[4] V. Hannstein, M. Behler, F. Sommer, *International Conference on Mathematics & Computational Methods Applied to Nuclear Science & Engineering*, **2017**.
[5] GNS, “Product information CASTOR V/52”, accessed Apr. 04, **2022**, https://www.gns.de/language=en/21553/castor-v-52.
[6] G. Spykman, *Nuclear Engineering and Technology* **2018**, *50*, 313.
[7] P. A. Raynaud, R. E. Einziger, *Journal of Nuclear Materials* **2015**, *464*, 304.
[8] Hummelsheim K., Rowold F., Kaufholz P., Behler M., Neles J., Spieth-Achtnich A., Völzke H., Spykman G., GRS-A-3984 (in German), GRS, **2019**.
[9] P.-C. A. Simon, C. Frank, L.-Q. Chen, M. R. Daymond, M. R. Tonks, A. T. Motta, *Journal of Nuclear Materials* **2021**, *547*, 152817.
[10] F. Boldt, *Journal of Nuclear Engineering and Radiation Science* **2019**, *5,* 020904.
[11] H. Sonnenburg, *Proceedings of the 49th Annual Meeting on Nuclear Technology* **2018**, 347.
[12] P. Konarski, C. Cozzo, G. Khvostov, H. Ferroukhi, *Journal of Nuclear Materials* **2021**, *555*, 153138.